PCCP

Structural Determination of Zn2+, Cu2+, and Fe2+ Complexed with Glutathione by IRMPD Spectroscopy and Complimentary ab Initio Calculations

Journal:	*Physical Chemistry Chemical Physics*
Manuscript ID	CP-ART-10-2024-003848.R1
Article Type:	Paper
Date Submitted by the Author:	08-Nov-2024
Complete List of Authors:	Walker, Samantha; University of Utah, Department of Chemistry Bubas, Amanda; University of Utah, Department of Chemistry Stevenson, Brandon; University of Utah, Chemistry Perez, Evan; University of Utah, Department of Chemistry Berden, Giel; Radboud University, Institute for Molecules and Materials Martens, Jonathan; Radboud Universiteit Nijmegen, Institute for Molecules and Materials, Felix Laboratory Oomens, Jos; Radboud University Nijmegen, Institute for Molecules and Materials Armentrout, Peter; University of Utah, Chemistry

Structural Determination of Zn^{2+}, Cu^{2+}, and Fe^{2+} Complexed with Glutathione by IRMPD Spectroscopy and Complimentary ab Initio Calculations

*Samantha K. Walker,[1,†] Amanda R. Bubas,[1,†,‡] Brandon C. Stevenson,[1] Evan H. Perez,[1] Giel Berden,[2] Jonathan Martens,[2] Jos Oomens,[2,3] and P. B. Armentrout[1]**

[1]Department of Chemistry, University of Utah, Salt Lake City, UT 84112-0850 USA

[2]Radboud University, Institute for Molecules and Materials, FELIX Laboratory, Toernooiveld 7, 6525 ED Nijmegen, The Netherlands

[3]van't Hoff Institute for Molecular Sciences, University of Amsterdam, Science Park 904, 1098 XH Amsterdam, The Netherlands

[†]These authors contributed equally as co-first authors.

[‡]*Present address: Pacific Northwest National Laboratory, Richland, WA 99352.*

ABSTRACT: Glutathione is a biologically abundant and redox active tripeptide that serves to protect cells from oxidative stress and rid the body of toxic heavy metals. The present study examines the coordination complexes of glutathione (GSH) with metals that are central to redox processes in biology, Zn, Cu, and Fe, using infrared multiple photon dissociation (IRMPD) action spectroscopy with a free electron laser. For all three metals, a complex between the metal dication and deprotonated GSH was formed, $M(GSH-H)^+$. The experimental IRMPD spectra were compared to scaled harmonic vibrational spectra calculated at the MP2/6-311+G(d,p) level of theory after thorough exploration of conformational space using a simulated annealing protocol. Interestingly, spectra calculated at the B3LYP or ωB97XD level do not match experiment as well. These findings offer the first gas-phase spectroscopic evidence for how the biologically relevant metal ions coordinate with glutathione. There are spectral features that are common to all three metals, however, noting the differences in the strengths of the common features between the three metals enables an assessment of the preference or specificity that each individual metal has for a given coordination site. Additionally, all three metals form structures where the deprotonated thiol of the cysteine side chain coordinates with the metal center, which is consistent with the involvement of the thiol site in biologically relevant redox chemistry.

INTRODUCTION

Glutathione (L-γ-glutamyl-L-cysteinylglycine, GSH) is a biologically abundant tripeptide that is involved in many biological processes, including protein synthesis, DNA synthesis, enzyme activity, metabolism, and defense of cells against oxidative stress.[1-2] When GSH is deactivated by the formation of a disulfide bridge between two oxidized GSH molecules forming GSSG or simply of limited availability, the ability of GSH to respond to oxidative stress within the body is decreased. Failure to respond and mitigate cellular oxidative stress has been linked to a number of diseases[3] including Wilson's disease[4] and Parkinson's disease.[5] Patients with Wilson's disease have low levels of reduced glutathione, and as a result, the concentration of copper in their blood is too high leading to organ damage.[4] For patients with Parkinson's disease, the iron concentration in the substantia nigra within the brain is elevated.[5] Increased iron concentration becomes problematic because Fe can generate hydroxyl radicals, inducing oxidative stress upon cells. The redox chemistry of GSH mitigates the effects of oxidative stress by reducing redox active metals and reactive oxygen species, including hydroxyl radicals, or by binding to heavy metals for subsequent elimination from the body.[6-8]

Several studies have shared the objective of obtaining structural information related to the coordination of metals to glutathione to ultimately elucidate the mechanism by which glutathione works to restore and maintain homeostasis.[9-14] These studies reveal that Zn and Cu, along with other heavy metals such as Cd, Pb, and Hg preferentially bind to the thiol site, whereas Fe coordinates with carboxylate sites. Although biologically relevant, many of these studies were carried out in solution, where the structure of the species under investigation is influenced by interactions with the solvent (for example, extensive hydrogen bonding networks and hydration of the metal center) and is highly sensitive to the pH conditions used in the study. Gas-phase experiments offer the opportunity to study metal-glutathione complexes free of solvent effects to reveal the intrinsic binding characteristics between glutathione and metal dications. Bohme and coworkers[15] previously investigated the dissociation pathways of deprotonated glutathione complexed with Co^{2+}, Ni^{2+}, Cu^{2+}, and Zn^{2+}. Their study suggests that these metals preferentially

bind to the thiol site of the cysteine side chain, and it was presumed that the C-terminus was deprotonated. Upon dissociation, the oxidation states of Co, Ni, and Zn do not change. In contrast, the Cu^{2+} radical in the copper complex can be reduced to Cu^{+} upon dissociation. This reduction can lead to more insidious implications in radical formation that leads to DNA damage in biological systems.

Previous IRMPD studies have examined protonated GSH and its S-nitroso derivative,[16] demonstrating that gas-phase GSH forms intramolecular hydrogen bonds that reduce the complexity and flexibility observed for GSH in solution. The spectroscopic study presented here focuses on the coordination chemistry of deprotonated glutathione with biologically relevant, metals that are central to redox processes in biology: zinc, copper, and iron. Notably, copper and iron are redox-active, whereas zinc(II) is redox-inert; however, zinc(II) has been demonstrated to have a central role in the control of redox biology.[17] To elucidate the site of deprotonation in forming the $M(GSH-H)^{+}$ species under investigation, it is worthwhile to consider the pK_a values of the active sites within glutathione. In the simplest considerations, the pK_a values for sites within the individual amino acids are as follows: pK_a (Glu N-terminal amino site) = 9.60, pK_a (Glu C-terminus) = 2.19, pK_a (Cys thiol side chain) = 8.18, pK_a (Gly C-terminus) = 2.34.[18] (The pK_a values of the Glu side chain and Cys C-terminus are not included here as they are involved in GSH backbone formation. Likewise, the Cys and Gly amino sites, pK_a = 10.28 and 9.60, respectively, are converted to amide sites, which in general, are mildly acidic.) Importantly, because acid/base chemistry trends in the gas phase are the reverse of what is reported in solution,[19-20] we anticipate that the common deprotonation sites for the $M(GSH-H)^{+}$ complexes will include the N-terminus and thiol site, and given the conclusions of Bohme and coworkers,[15] we also consider deprotonation at both carboxylic acids. Additionally, we anticipate that deprotonation of the thiol site (creating the anionic S^{-} moiety) creates a strong M^{2+} binding site, which is directly comparable to observations from solution-phase studies. The present study conducted in the absence of solvent interactions may shed light on other favorable metal coordination sites within GSH that might provide more detail related to the mechanism by which GSH manages oxidative stress in biological

systems. Several previous studies have successfully employed infrared multiple photon dissociation (IRMPD) action spectroscopy to obtain structural information for a wide range of systems[21] including biological molecules[22-28] and metal-cationized biological molecules,[29-34] for instance, amino acids,[25, 35-62] dipeptides,[63-65] tripeptides,[66-68] and amino-acid based dimers.[69-70] The success of these previous IRMPD studies of metalated peptides provides a strong foundation to support the current study of the metalated tripeptide, GSH.

METHODS

Sample Preparation

Solutions were prepared by dissolving glutathione (Sigma-Aldrich) and the respective metal dichloride, Zn, Cu, and Fe (Sigma-Aldrich), in 50:50 H_2O:acetonitrile. These solutions were further diluted in methanol to 10^{-5} M concentrations for use in the electrospray ionization (ESI) source and mass isolated for subsequent IRMPD experiments. For all three metals, the primary complexes formed were singly charged combinations of the metal dication with deprotonated glutathione, designated as $M(GSH-H)^+$ hereafter.

IRMPD Experiment

Experiments were carried out using the ion trap instrument coupled to the beamline of the Free Electron Laser for Infrared eXperiments (FELIX) at Radboud University, The Netherlands.[71] The details of the full experimental setup have been described previously.[72] The FEL was scanned over the 700 to 1900 cm^{-1} region and operated at a 10 Hz macropulse repetition rate with a maximum pulse energy of 50 mJ. Spectra shown below include only 1000 – 1900 cm^{-1} because no peaks were observed in the 700 – 1000 cm^{-1} range. The full experimental spectra are shown in Figures S1 – S3. The 700 – 1900 cm^{-1} range was examined spectroscopically because previous studies of similar systems have shown this to be a region where the most characteristic peaks are observed and this was the optimized range for these experiments during the available beamtime. Calculations indicate that peaks from 300 – 700 cm^{-1} are generally low in intensity and not particularly distinctive, see Figures S4 – S6. The trapped ions were irradiated with a single

macropulse that was attenuated in order to prevent excessive ion depletion (saturation).[73] The IRMPD spectra shown here were generated by plotting the photofragmentation yield, $Y = -\ln[\Sigma I_p/(\Sigma I_F + \Sigma I_P)]$, where I_F and I_P are the integrated intensities of the fragment and precursor mass peaks, respectively, as a function of the frequency of IR radiation. The yield was corrected for frequency-dependent variation in the laser pulse energy. These corrections are appropriate for this experiment because the power dependence of the dissociation is practically linear until saturation occurs because of the incoherent nature of the multiple photon excitation process, a phenomenon well detailed in the literature.[73-74]

Computational Details

A simulated annealing program explained in greater detail previously[75-80] along with two structures from a previous computational study[81] of Co(GSH-H)$^+$ were used to identify low-energy structures for the Zn(GSH-H)$^+$ complexes. It is important to realize that to provide comprehensive structural coverage the simulated annealing protocol must start with structures where the proton has been removed from several different sites and where the iminol structures discussed below are explicitly considered. Briefly, our simulated annealing procedure employs the Amber force field[79-80] to generate unique structures followed by geometry optimizations at the B3LYP/6-31G(d)[82-83] level of theory using the Gaussian16[84] software package. These geometries were then used as starting points for the Cu(GSH-H)$^+$ and Fe(GSH-H)$^+$ systems. Spin states considered for these three systems were singlet for Zn, doublet for Cu, and singlet, triplet, and quintet for Fe. For Fe, structures with a singlet and triplet spin state were found to lie higher in energy than the quintet states and are not discussed further. These structures and additional higher energy structures for all systems are instead listed in the Supplementary Information, Table S1. The geometries of low-energy structures (energies less than 0.02 Hartrees with respect to the lowest energy species as calculated at the B3LYP/6-31G(d) level) were optimized using B3LYP/6-311+G(d,p) within the Gaussian16[84] software package. Additionally, structures of selected species were optimized with MP2[85]/6-311+G(d,p). Before comparison with experimental spectra, harmonic vibrational frequencies calculated for the optimized structures at the B3LYP and MP2 levels were scaled by

0.975 and 0.965, respectively. This scaling factor for B3LYP has been shown to accurately reproduce IRMPD spectra of related molecules in previous studies.[24-28, 41, 44, 46-48, 50, 52-62, 65, 70] The MP2 scaling factor was chosen such that the carbonyl stretch was reproduced, and this was consistent for all three metal systems, see below. A Gaussian line shape (FWHM = 25 cm^{-1}) was used to broaden the calculated vibrational spectra for comparison to the IRMPD spectra.[86] This FWHM accounts for the finite laser bandwidth and unresolved rotational structures. When comparing theoretical calculated spectra to experimental spectra, it is important to note that the intensities may differ because the calculated spectra correspond to a single-photon process whereas acquisition of the IRMPD spectra require the absorption of multiple IR photons of resonant wavelength to induce dissociation. Vibrational assignments provided below were based on the predicted vibrational character and are included next to the wavenumber of the experimental band in parenthesis.

Single point energy (SPE) calculations for the B3LYP optimized structures were performed using the 6-311+G(2d,2p) basis set with the B3LYP, ωB97XD,[87] and MP2(full), where full indicates correlation of all electrons, levels of theory. Zero-point energy (ZPE) corrections and 298 K thermal corrections using frequencies calculated at the B3LYP/6-311+G(d,p) or MP2/6-311+G(d,p) level, as indicated, were applied to SPEs to provide the relative enthalpies at 0 K and Gibbs energies at 298 K. Vibrational frequencies used for ZPE and thermal corrections were scaled by 0.9896.[88] In select cases, we also performed CCSD(T)/6-311+G(d,p)//MP2/6-311+G(d,p) single point calculations. Structures were also optimized using the B3LYP-GD3BJ[89-90] level of theory using the 6-311+G(d,p) basis set to assess the influence of dispersion forces on energies and structures. These structures were then used to calculate SPEs including the GD3BJ dispersion corrections using the larger 6-311+G(2d,2p) basis set.

RESULTS AND DISCUSSION

Nomenclature

Glutathione is a unique tripeptide in that it is not composed of three amino acids bound by traditional peptide bonds. In glutathione, glutamic acid forms a gamma peptide linkage to cysteinylglycine through an amide bond between the carboxylic acid carbon of the glutamic acid side chain and the amino group of the cysteine residue. To provide a thorough description of how the metal coordinates with glutathione, we label the various heteroatoms of GSH as shown in Figure 1. Here, we denote the amino nitrogen of the glutamic acid residue as N^1, the amide nitrogen of the cysteine residue as N^2H, and the amide nitrogen of glycine as N^3H (not shown). When the hydrogen originally on N has migrated to a nearby oxygen atom of a carbonyl group to form an iminol group, the iminol nitrogen of the cysteine residue is denoted as N^2 (not shown) and the iminol nitrogen of glycine as N^3. (Note that the iminol motif shown here is uncommon in bare GSH and tautomerization to such a structure is driven by metal complexation.[9, 91]) To address the fact that there is a glutamyl gamma bond to cysteinylglycine, we denote the carbonyl of the side chain of the glutamic acid as CO^γ and refer to the backbone carboxylic acid of glutamic acid as CO^1, the backbone carbonyl of the cysteine residue as CO^2, and the backbone carbonyl of glycine as CO^3. In instances where the peptide linkage is in the iminol tautomeric form, the carbonyl where the proton has migrated is denoted as $CO^\gamma H$ (not shown) or CO^2H, corresponding to either the glutamyl gamma carbonyl or the cysteine carbonyl, respectively. The thiol side chain of the cysteine residue is referred to as S unless the tripeptide is deprotonated at that site, in which case it is denoted as S^- (not shown). The description of which sites bind to the metal is provided in square brackets. Table S2 in the Supplementary Information also includes a designation of the dihedral angles along the backbone of the deprotonated GSH ligand. Additionally, Table 1 compares the metal-ligand bond distances for each of the systems discussed here.

Comparison of Zn (GSH-H)$^+$, Cu(GSH-H)$^+$, and Fe(GSH-H)$^+$ Spectra

A comparison of the experimental IRMPD spectra of the Fe(GSH-H)$^+$, Cu(GSH-H)$^+$, and Zn(GSH-H)$^+$ complexes is shown in Figure 2. All M(GSH-H)$^+$ complexes possess strong spectral features near 1685 (CO^3 and CO^γ stretches), 1617 (N^1H_2 scissor and CO^γ stretch), and 1425 cm^{-1} (CO^3H in-plane bend and CH_2 scissor). Zn(GSH-H)$^+$ possesses a strong feature at 1763 cm^{-1} (CO^1

stretch) that becomes less pronounced in the $Cu(GSH-H)^+$ spectrum and is absent in the $Fe(GSH-H)^+$ spectrum. As will be discussed below, this feature is associated with the CO stretch of an uncoordinated carboxylic acid, indicating that the Zn and Cu complexes possess a free carboxylic acid site, whereas Fe coordinates with both carboxylic acid sites, in agreement with the previous solution phase study where Fe shows a clear preference for coordination with carboxylate donor sites.[14] A feature near 1500 cm^{-1} (CO^3H and CN^2H in-plane bend) is a minor feature for the $Zn(GSH-H)^+$ species, more prominent and red shifted for the Cu analogue, and strongest for the Fe analogue. The feature in the Zn spectrum near 1147 cm^{-1} (uncomplexed carboxylic acid COH in-plane bend) decreases in intensity and blueshifts as one works across the row from the zinc to the copper to the iron system. This is an experimental indication of variations in the metal binding to the carboxylic acid groups. $Zn(GSH-H)^+$ has a strong, characteristic feature at 1073 cm^{-1} (N^1H_2 wag) that is possibly shifted for the Cu complex and weakest for the Fe complex. Each of the $M(GSH-H)^+$ spectra also possess bands near 1230 cm^{-1} (N^1H_2 twist and predominantly CN^2H and CN^3H in-plane bends) and 1280 cm^{-1} (backbone CH_2 and N^1H_2 twists). Each of the $M(GSH-H)^+$ spectra have a peak labelled v^9, however all these peaks correspond to different vibrations. All vibrations listed here are labelled in Figure 2 and identified further in Tables S6, S7, and S8 for the Zn, Cu, and Fe complexes, respectively.

Relative Energies and Structures of $Zn(GSH-H)^+$

The relative energies of low-lying $Zn(GSH-H)^+$ structures identified through simulated annealing and calculated using the B3LYP//B3LYP, B3LYP-GD3BJ//B3LYP-GD3BJ, and ωB97XD//MP2 density functionals and MP2(full)//MP2 level of theory are detailed in Table S3. The lowest energy structures of each of the four unique metal coordination motifs are shown in Figure 3. Notably, although the energies differ, the B3LYP and B3LYP-GD3BJ calculations converge to nearly identical structures, whereas the MP2 structures show some distinct differences, as detailed below. The calculated global minimum (GM) at all levels of theory is [N^1, CO^γ, S^-, CO^3], which coordinates the Zn^{2+} with the N-terminus and gamma carbonyl of the glutamic acid. The thiol site is deprotonated, as expected on the basis of pK_a considerations, and the sulfur

coordinates with the metal along with the C-terminal carbonyl. The [N^1, CO^1, CO^γ, CO^{3-}] structure lies 4 - 8 kJ/mol above the GM at 298 K and again coordinates Zn^{2+} with the N-terminus and gamma carbonyl of the glutamic acid. The backbone carbonyl of the glutamic acid, CO^1, is rotated into the metal binding pocket. The thiol site is protonated and therefore is oriented away from the metal. Instead, the C-terminus is deprotonated, and the metal coordinates with one of the C-terminal oxygen sites. The [CO^1, CO^γ, S^-, CO^3] structure is similar to the GM, but for this species, the CO^1 group of the N-terminus binds to the metal in place of the N^1 amino group. This exchange of glutamic acid backbone coordination sites results from the rotation of one dihedral angle and increases the energy of the complex by 5 – 17 kJ/mol relative to the GM. The [N^1, CO^1, N^2H, S^-] structure coordinates the Zn^{2+} with the N-terminus, the CO^1 carbonyl, the amine backbone nitrogen, and the deprotonated thiol site. (This is one of the structures identified for $Co(GSH-H)^+$ by Spezia et al.[81]) This structure lies 13 – 16 kJ/mol above the GM at most levels of theory; however, B3LYP suggests that it is nearly isoenergetic with the GM. For the $Zn(GSH-H)^+$ system, iminol structures lie higher in energy than their amide counterparts by 3 – 21 kJ/mol (Table S2). This contrasts with previous IRMPD investigations of the structures of metalated tripeptides,[68, 92] which indicated that iminol type structures can lie lower in energy than their amide counterparts, such that they are experimentally present. However, in these previous studies, the peptide was not deprotonated and the complex retained a charge of 2+.

IRMPD spectrum of $Zn(GSH-H)^+$

The photodissociation spectrum of $Zn(GSH-H)^+$ is shown in Figure 3. Major spectral features are located at 1763, 1688, 1620, 1543, 1499, 1426, 1284 (broad), 1231, 1147, and 1073 cm^{-1}. Spectra calculated at the MP2/6-311+G(d,p) level for the GM structure and for the lowest-energy conformations for each of the other three unique metal chelation structures are also shown in Figure 3. The predicted GM at all levels of theory, [N^1, CO^γ, S^-, CO^3], has a calculated spectrum that reproduces the experimental spectrum remarkably well, both in terms of the locations and intensities of the bands. The calculated spectrum for the GM possesses features at 1752 (CO^1 stretch), 1724 (CO^2 stretch), 1683 (CO^3 stretch), 1605 (CO^γ stretch), 1544 (CN^2H in-plane bend),

1510 (CN^3H in-plane bend), 1425 (C-terminus in-plane COH bend), 1364 (CO^1H in-plane bend), 1303 (CO^3H in-plane bend), 1253 (CH_2 twists), 1221 (N^1H_2 twist and CN^2H and CN^3H in-plane bends), 1176 (CO^3H in-plane bend), 1163 (N^1H_2 wag), 1149 (CO^1H in-plane bend), 1089 (CC backbone stretch), and 1071 cm^{-1} (N^1C stretch). Arguably, the calculated spectrum for the GM structure does not capture the intensities of the bands observed at 1231 and 1073 cm^{-1}. However, the intensity of the 1073 cm^{-1} band may have been artificially enhanced because it is positioned to the red of a strong absorption band, which is a well-known and documented artifact of IRMPD spectroscopy.[93] The spectra shown in Figure 3 were calculated at the MP2/6-311+G(d,p) level of theory, and although MP2 is more computationally expensive than the B3LYP/6-311+G(d,p) and ωB97XD/6-311+G(d,p) DFT methods, the DFT methods do not adequately reproduce the CO^3 carbonyl stretch at 1688 cm^{-1} or the bands observed at 1426 and 1073 cm^{-1}, see Figure S4. The MP2 calculations suggest that Zn^{2+} binds tightly to GSH as the bond lengths between Zn^{2+} and the GSH coordination sites are ~0.03 Å shorter in the MP2 structure than in the B3LYP structure.

The spectrum for the [N^1, CO^1, CO^γ, CO^{3-}] structure possesses features that reproduce a few of the experimental bands well with features at 1689 (CO^1, CO^2, and CO^{3-} stretches), 1610 (CO^γ stretch), 1228 (CSH in-plane bend and CH_2 twist), and 1080 cm^{-1} (N^1H_2 wag). However, this spectrum overestimates the intensity of the band at 1532 cm^{-1} (CN^2 stretch) and does not capture the experimentally observed features at 1763, 1426, and 1147 cm^{-1}.

The spectrum for the [CO^1, CO^γ, S^-, CO^3] structure reproduces the features at 1688, 1620, and 1426 cm^{-1} but fails to capture the major features at 1763, 1147, and 1073 cm^{-1}. The spectrum for the [N^1, CO^1, N^2H, S^-] species approximates many of the experimental bands with vibrations at 1757 (CO^3 stretch), 1726 (CO^γ stretch), 1690 (CO^1 stretch), 1421 (CO^1H in-plane bend), and 1396 and 1155 (CO^3H in-plane bends), and 1105 cm^{-1} (N^1H_2 wag). This spectrum does not reproduce the major features observed at 1620, 1284, 1231, and 1073 cm^{-1} and is unlikely to be a major contributor to the experimental spectrum.

The comparison of the locations and intensities of the calculated spectral features with those contained in the experimental spectrum convincingly suggests that the GM structure,

[N^1, CO^γ, S^-, CO^3], is the primary contributor to the experimental spectrum. The [N^1, CO^1, CO^γ, CO^{3-}], [CO^1, CO^γ, S^-, CO^3], and [N^1, CO^1, N^2H, S^-] structures may be present, although they are not necessary to reproduce the experimental spectrum.

Relative Energies and Structures of Cu(GSH-H)$^+$

The relative energies of four unique Cu(GSH-H)$^+$ chelation structures are provided in Table S4 and shown in Figure 4. Again, B3LYP and B3LYP-GD3BJ calculations converge to very similar structures. The [N^1, CO^1, N^2H, S^-] structure is predicted to be the 298 K GM for all levels of theory except for MP2, where it is 30 kJ/mol above the MP2 GM at 298 K, [N^1, CO^γ, S^-, N^3H, CO^3]. To further explore this discrepancy, we also calculated CCSD(T)/6-311+G(d,p)//MP2/6-311+G(d,p) Gibbs energies at 298 K, finding that the former structure lies 11 kJ/mol above the latter. The [N^1, CO^1, N^2H, S^-] structure utilizes the N-terminus and CO^1 group to coordinate Cu^{2+}. The thiol site is deprotonated, as anticipated based on pK_a considerations mentioned above, and is therefore available as a metal coordination site. The [N^1, S^-, CO^2] structure is 6 – 22 kJ/mol higher in energy than the GM. This ostensibly tri-dentate coordination probably also has a Cu interaction with N^2, although the Cu-N^2 distance is 2.49 Å, which is slightly longer than that in the GM [N^1, CO^1, N^2H, S^-] structure, where the Cu-N^2 distance is 2.22 Å. (It can be noted that a key difference between the structures obtained by B3LYP and MP2 is the Cu-N^2 bond distance, 2.22 Å for MP2 but 2.85 Å for B3LYP, which leads to several vibrational bands shifting appreciably.) The [N^1, CO^γ, S^-, N^3H, CO^3] structure is the MP2 and CCSD(T) 298 K GM, whereas other levels of theory calculate this structure to be 14 – 57 kJ/mol higher in energy with respect to their GM. Here, the B3LYP and MP2 structures differ much less in the Cu-N^3 interaction, with bond lengths of 2.20 Å and 2.10 Å, respectively. Note that a [N^1, CO^γ, S^-, CO^3] structure was identified as the GM for the Zn^{2+} system, where there is essentially no interaction with N^3H with a Zn-N^3 distance of 2.85 Å (3.01 Å in the B3LYP structure). Lastly, the [N^1, CO^1, N^2, S^-, CO^2] structure is 20 – 51 kJ mol higher in energy with respect to the GM. This structure coordinates Cu^{2+} with the N-terminus, the carbonyl of the carboxylic acid of glutamic acid, the iminol tautomerized peptide linkage N^2, the deprotonated thiol, and the backbone carbonyl of the cysteine residue. Because the C-terminus is

not involved in binding, this section of the molecule is oriented away from Cu^{2+}, leading to a less compact structure. The stability of this structure is consistent with a previous IRMPD study of a Cu coordinated histidine dipeptide, which indicated that Cu^{2+} forms low-energy pentadentate structures using a similar theoretical treatment as the approach used here.[65]

IRMPD spectrum of $Cu(GSH-H)^+$

The photodissociation spectrum of $Cu(GSH-H)^+$ is shown in Figure 4. Major spectral peaks are centered at 1770, 1685, 1587, 1505, 1423, 1246, 1159, and 1102 cm^{-1}. Spectra calculated at the MP2/6-311+G(d,p) level for the lowest-energy conformations of each unique metal chelation structure are also shown in Figure 4. The [N^1, CO^1, N^2H, S^-] structure is the GM at all levels of theory except for MP2 and CCSD(T) and has a calculated spectrum that reproduces the experimental spectrum fairly well with bands predicted at 1757 (CO^3 stretch), 1684 (CO^γ stretch), 1675 (CO^1 stretch), 1589 (N^1H_2 scissor), 1514 (CN^3H in-plane bend), 1395 (CO^3H in-plane bend), 1275 (CO^3H in-plane bend and CH_2 wag), 1155 (CO^3H in-plane bend), and 1097 cm^{-1} (N^1H_2 wag). This spectrum does not reproduce the intensities of the bands at 1587 and 1246 cm^{-1}. Here, the B3LYP and MP2 (shown) spectra are more similar, Figure S5, although the MP2 spectrum reproduces the bands observed at 1505 and 1102 cm^{-1} better than the B3LYP spectrum. In contrast to the Zn complex, the bond lengths between the metal and the complexation sites are more comparable (0.005 Å smaller for MP2) for N^1, CO^1, and S^-; however, as noted above, the interaction between Cu and N^2Although the [N^1, S^-, CO^2] structure captures the location of the 1770, 1159, and 1102 cm^{-1} peaks with calculated bands at 1777 (CO^1 stretch), 1761 (CO^3 stretch), 1159 (CO^3H in-plane bend), and 1086 cm^{-1} (N^3C stretch), it does not sufficiently reproduce the intensities of the experimentally observed bands, it fails to capture major peaks from 1200 – 1750 cm^{-1}, and it overestimates the intensities of the bands at 1330 and 1650 cm^{-1}.

The [N^1, CO^γ, S^-, N^3H, CO^3] structure is the MP2 and CCSD(T) GM and has a calculated spectrum that reproduces most features in the experimental spectrum with bands predicted at 1759 (CO^2 stretch), 1749 (CO^1 stretch), 1695 (CO^3 stretch and CO^3H in-plane bend), 1620 (CO^γ stretch), 1581 (N^1H_2 scissor), 1529 (CN^2H in-plane bend), 1441 (CO^3H in-plane bend and nearby NH_2

wag), 1362 (CO^1H in-plane bend), 1303 (CO^3H in-plane bend), 1178 (CO^3H in-plane bend), 1148 (CO^1H in-plane bend), 1107 (CN^3 stretch), and 1091 and 1071 cm^{-1} (CN^1 stretches). However, the predicted spectrum for the [N^1, CO^γ, S^-, N^3H, CO^3] structure overestimates the intensity of the peak at 1770 cm^{-1} and underestimates the intensities of the features at 1587, 1505, and 1246 cm^{-1}, which could suggest that one or more additional isomers contribute to the experimental spectrum. Here, the B3LYP and MP2 spectra are similar (Figure S5), and the B3LYP spectrum reproduces the bands at 1423 and 1159 cm^{-1} but also predicts a band at 1058 cm^{-1} that is not observed in the experimental spectrum. The bond lengths between Cu^{2+} and each of the GSH coordination sites in the MP2 structure are ~0.05 Å shorter than those in the B3LYP structure except for the Cu-N^3H bond, which is 0.09 Å shorter.

The calculated spectrum for the [N^1, CO^1, N^2, S^-, CO^2] structure possesses features at 1759 (CO^3 stretch), 1701 and 1688 (CO^1 and CN^2 stretches), 1634 (CO^2 stretch), 1534 (CN^3H in-plane bend), 1447 (CH_2 scissor), 1403 (CO^3H in-plane bend), 1327 (cysteine CH bend), 1296 ($CO^\gamma H$ in-plane bend), 1263 ($CO^\gamma H$ in-plane bend), 1158 (CO^3H in-plane bend), 1098 (N^3C stretch and CO^3H in-plane bend), and 1068 cm^{-1} (N^1H_2 wag). This spectrum reproduces the features at 1770, 1246, 1159, and 1102 cm^{-1} in the experimental spectrum; however, the calculated spectrum for this pentadentate species does not capture the locations or intensities of the features in the 1400 to 1700 cm^{-1} range, and the predicted 1036 cm^{-1} band is not observed.

We conclude that the calculated GMs, [N^1, CO^1, N^2H, S^-] and [N^1, CO^γ, S^-, N^3H, CO^3], are likely to be present and contribute to the experimental spectrum.

Relative Energies and Structures of $Fe(GSH-H)^+$

The relative energies of the unique $Fe(GSH-H)^+$ chelation structures with a quintet spin state, calculated using the B3LYP//B3LYP, B3LYP-GD3BJ//B3LYP-GD3BJ, and ωB97XD//MP2 density functionals and MP2(full)//MP2 level of theory are detailed in Table S5. Their structures and energies are displayed in Figure 5. B3LYP and B3LYP-GD3BJ calculations converge to nearly identical structures. Most of the structures were reproduced at all three multiplicities except for one higher-energy structure that was unstable with a quintet multiplicity.

In all cases, the triplet and singlet spin states produce structures that are higher in energy by more than 103 and 141 kJ/mol, respectively, with some differences in the relative energetic ordering of the different structures.

The GM at all levels of theory for $Fe(GSH-H)^+$ is [CO^1, S^-, CO^2, CO^3], a four-coordinate structure. The peptide wraps around the metal ion and represents a charge solvated (CS) structure. In this structure, GSH is deprotonated at the thiol group, as predicted by the comparison of pK_a values for the functional GSH sites, which provides a strong coordination site for Fe^{2+}. The [CO^1, CO^γ, S^-, CO^3] structure lies 9 – 17 kJ/mol above the GM at 298 K and is structurally similar with three of the four binding sites being the same, including the deprotonated sulfur. The energy difference is the result of a backbone rotation that orients the CO^2 group outward and rotates the CO^γ group into the metal binding pocket. At the MP2 level, this structure also appears to have a weak Fe-N^3H interaction characterized by a bond length of 2.49 Å and an HNCO dihedral angle of 153°. This is absent in the B3LYP geometry where the bond length is 3.12 Å and the dihedral is 175°. Because of the energetic proximity of these two structures, we also calculated their relative 298 K Gibbs energies at the CCSD(T)/6-311+G(d,p)//MP2/6-311+G(d,p) level finding that [CO^1, CO^γ, S^-, CO^3] remains higher in energy by 15 kJ/mol. The [N^1, CO^1, N^2, S^-, CO^2] structure lies 11 – 50 kJ/mol above the GM at 298 K. This structure is an iminol that coordinates the N-terminus and the deprotonated thiol, however, the proton originally on the N^2H group migrates to the CO^γ group, allowing the N^2 atom to bind to the metal. The [N^1, N^2H, S^-, CO^2] structure lies 20 – 52 kJ/mol above the GM. In this structure, the N-terminus, deprotonated thiol, and the CO^2 groups coordinate with the metal. Here, we also assign the N^2H as occupying a coordination position given the Fe-N^2 bond distance of 2.29 Å, only slightly elongated compared to the Cu-N^2 bond distance in the B3LYP GM of 2.22 Å.

IRMPD spectrum of $Fe(GSH-H)^+$

The photodissociation spectrum of $Fe(GSH-H)^+$ is shown in Figure 5. Major spectral features are centered at 1685, 1602, 1517, 1425, 1263, 1219, 1162, and 1040 cm^{-1}. Spectra calculated at the MP2/6-311+G(d,p) level for the quintet spin complexes are overlaid with the

experimental spectrum in Figure 5. The calculated spectrum for the GM, [CO^1, S^-, CO^2, CO^3], possesses features at 1709 (CO^1, CO^2, and CO^3 stretches), 1696 (CO^γ stretch), 1667 (CO^1 stretch), 1608 (CO^2 stretch), 1599 (N^1H scissor), 1536 (CN^3H in-plane bend), 1488 (CN^2H in-plane bend), 1461 (CO^1H in-plane bend), 1307 (CO^3H in-plane bend and nearby CH_2 wag), 1269 (CO^1H in-plane bend and nearby CH bend), and 1177 cm^{-1} (CO^3H in-plane bend), which correspond well with the positions of major spectral features in the experimental spectrum except for the intense band at 1461 cm^{-1}. However, the spectrum for the GM does not reproduce the intensities of the bands observed at 1517, 1263, and 1219 cm^{-1}. The B3LYP spectrum for this species is similar to that shown for MP2 but does a poorer job of reproducing the bands at 1602 and 1040 cm^{-1}, see Figure S6. In the MP2 calculated spectrum, the band at 1461 cm^{-1} has red-shifted to overlap better with the experimentally observed band at 1425 cm^{-1}, although its intensity is still too large. The only appreciable difference between the MP2 and B3LYP [CO^1, S^-, CO^2, CO^3] structures is the Fe-S bond length, which is 0.02 Å shorter in the B3LYP structure.

Because the [CO^1, CO^γ, S^-, CO^3] structure is reasonably low in energy at most levels of theory, it is possible that this structure is present and contributes to the experimental spectrum. The calculated spectrum for the [CO^1, CO^γ, S^-, CO^3] structure is similar to that of the GM and includes features at 1735 (CO^2 stretch), 1713 and 1688 (CO^1 and CO^3 stretches), 1608 (CO^γ stretch), 1595 (N^1H_2 scissor), 1545 (CN^2H in-plane bend), 1461 (CN^3H in-plane bend), 1433 (CO^1H in-plane bend), 1302 (CO^3H in-plane bend), 1181 (CO^3H in-plane bend), and 1154 and 1149 cm^{-1} (CN^3 stretch and C^1H_2 twist) that reproduce major features in the experimental spectrum. This spectrum nicely reproduces the shapes of the bands at 1685 cm^{-1} and 1425 cm^{-1}. Similar to the GM, the intensities of the bands observed at 1517, 1263, 1219, and 1162 cm^{-1} are not reproduced well, and the calculated spectrum does not reproduce the minor band observed at 1040 cm^{-1}. The B3LYP spectrum for this species is very similar to the MP2 spectrum in Figure 5 (see Figure S6) although the shape of the band at 1685 cm^{-1} is reproduced better by the MP2 spectrum. The structures calculated using MP2 and B3LYP are similar, but the bond lengths between Fe and the GSH coordination sites are 0.02 – 0.04 Å longer in the MP2 structure than in the B3LYP structure.

Interestingly, this is in contrast to the observations of MP2 with Zn and Cu, where the bond lengths are shorter than those obtained using B3LYP.

Both the [N^1, CO^1, N^2, S^-, CO^2] and [N^1, N^2H, S^-, CO^2] structures possess major features at 1759 (CO^3 stretch) and 1775 (CO^1 stretch) cm^{-1}, respectively, that do not correspond to features in the experimental spectrum. Therefore, we conclude that these two structures do not contribute to the experimental spectrum. (The latter structure was assigned as the global minimum structure for $Co(GSH-H)^+$ by Spezia et al.[81])

On the basis of spectroscopic matches, we conclude that the [CO^1, CO^γ, S^-, CO^3] and [CO^1, S^-, CO^2, CO^3] structures are the main contributors and present under the experimental conditions.

Comparison to solution phase studies

The [N^1, CO^γ, S^-, CO^3] GM structure identified for $Zn(GSH-H)^+$ indicates that the thiol site is deprotonated, resulting in Zn^{2+} coordination with the deprotonated thiol. Coordination of Zn^{2+} with the thiol site of GSH in the gas phase reflects solution phase observations where Zn^{2+} shows a clear preference for thiol binding sites.[14] The same solution-phase study indicates that Zn^{2+} will also bind with the N-terminus of GSH, as also reflected by our GM.

Overall, the energetic predictions for Cu^{2+} are not as clear-cut as those for the Zn^{2+} complex. The DFT methods identified [N^1, CO^1, N^2H, S^-] as the GM whereas MP2 identified [N^1, CO^γ, S^-, N^3H, CO^3] as the GM. However, the prevalence of low-lying structures where Cu^{2+} coordinates with the deprotonated thiol site aligns with solution-phase studies that also show Cu^{2+} coordinates with GSH at the thiol site.[11-12] Further, coordination of GSH with Cu(II) has been shown to be particularly important in mitigating metal-mediated oxidative damage to DNA, although adequate mitigation may occur by the involvement of a second GSH molecule to form the Cu(II)-GSSG complex.[12] Studies into the structure of the dimer, Cu(II)-GSSG may offer additional insight and help explain why there might be two low-energy structures for the monomer.

Our analysis of the Fe^{2+} system identified the [CO^1, CO^γ, S^-, CO^3] and [CO^1, S^-, CO^2, CO^3] structures as the main contributors to the experimental spectrum. Compared to the other metal

complexes examined here, these results are consistent with solution-phase observations that indicate Fe^{2+} binds preferentially with carboxylate donor sites along with the active deprotonated thiol site.

Our results indicate that the deprotonated thiol site of cysteine is active in metal binding, as anticipated on the basis of the redox activity of GSH in biological systems. Our results concur with solution phase studies that indicate Zn^{2+} binds with the thiol and N-terminus of GSH, Cu^{2+}, which is particularly insidious in causing oxidative stress, binds to the active thiol site, and Fe^{2+} coordinates with free carboxylates. Agreement between our results and those from solution-phase studies offers support that gas-phase studies may offer valuable structural information that can be applied to deduce mechanisms involved in biological processes.

Comparison to previous studies

Dunbar et al. investigated factors that may influence the preference of a metal for imidol (IM) and charge separated (CS) binding configurations using dialanine and trialanine[91] as model systems. They highlighted that the IM isomer is favored by factors such as increased metal ion charge, electrostatic interactions, and stronger ion binding. Dunbar introduced an electrostatic parameter, q/R (where q is ion charge and R is distance to chelation site), that scaled with the binding energies of "main-group" metals but was less reliable for "transition" metals. Additionally, factors such as metal hardness, peptide length (dipeptide vs. tripeptide), and number of chelation points were explored. However, Dunbar found that metal hardness and peptide length had minimal predictive ability, resulting in similar outcomes regardless of Lewis-basic chelation points available.

When considering the factors that affect metal ion – peptide binding configurations outlined in the previous work of Dunbar et al., we anticipated that IM structures would be identified as low-energy species for the complexes of Zn^{2+}, Cu^{2+}, and Fe^{2+} with deprotonated GSH. In contrast, Zn^{2+} IMs were higher in energy and not contributors to the experimental spectrum. Although all Cu^{2+} and Fe^{2+} complexes did have IM representation among the four low-energy unique structures, none of the iminol structures were identified as dominant contributors to the

experimental spectrum. Fe^{2+} is the metal that is closest to "borderline" character described by Dunbar et al., such that the prevalence of CS structures for the $Fe(GSH-H)^+$ complex is consistent with their predictions. The use of dialanine as a model peptide system provided a baseline for prediction of metal binding motifs in small, simple peptides; however, GSH is larger and more complex than dialanine or trialanine, has a gamma peptide linkage, and – likely most important – functionalized side chain sites that compete with the backbone amide linkages in metal binding. Consequently, the factors influencing metal-peptide bonding interactions identified by Dunbar are useful for peptides with aliphatic side chains but do not take into account the competition from Lewis basic sites in side chains of more complex peptides.

CONCLUSION

In previous work on similar metalated complexes,[25, 34, 36, 38-50, 52, 55-70] comparisons of B3LYP spectra with experimental IRMPD spectra were generally sufficient to identify the structures present with confidence. In the present work, we found that MP2 predicted spectra generally provided a superior reproduction of the experimental spectra. Although the differences in the theoretical spectra are subtle and the GSH molecule cannot be considered ideal, the strength of the metal binding interactions predicted by MP2 and density functional approaches lead to distinct changes in the frequencies of several bands in all three complexes examined here. Moving forward, this suggests that the more expensive MP2 calculations be considered for spectral identification in problematic systems.

Several spectral features are observed that are prevalent for each $M(GSH-H)^+$ complex. The features near 1685 (CN^2 and CO^γ stretches), 1617 (N^1H_2 scissor and CO^γ stretch), 1425 (CO^3H in-plane bend and CH_2 scissor), 1280 (backbone CH_2 twist and N^1H_2 twist), and 1230 (N^1H_2 twist, and predominantly CN^2H in-plane bend and CN^3H in-plane bend) cm^{-1} were observed for all three $M(GSH-H)^+$ complexes. The spectrum for the $Zn(GSH-H)^+$ complex possesses a strong feature at 1763 cm^{-1} that is weaker in the $Cu(GSH-H)^+$ spectrum and absent in the $Fe(GSH-H)^+$ spectrum. The feature at 1763 cm^{-1} is associated with the CO stretch of an uncoordinated CO^1 site,

demonstrating that Zn does not coordinate with this site, only a portion of Cu complexes do, and Fe *does* coordinate with the CO^1 and CO^3 sites, in agreement with observations that Fe preferentially coordinates with carboxylate sites noted in solution phase studies.[9-14] The feature at 1500 cm^{-1} (CO^3H and CN^2H in-plane bend) is a minor feature for the $Zn(GSH\text{-}H)^+$ species and is more intense for the $Cu(GSH\text{-}H)^+$ species and strongest for the $Fe(GSH\text{-}H)^+$ species, which is consistent with an increased preference for Fe^{2+} to coordinate more strongly with carboxylic acid sites. The feature near 1147 cm^{-1} (carboxylic acid CO^xH in-plane bend) decreases in intensity and blueshifts from the Zn to the Cu to the Fe system. This variation is associated with distinct modes: for Fe, this is indicative of coordination with CO^3; for Cu, coordination with CO^1; and for Zn, the CO^1 group does not coordinate with the metal. Although many of the spectral features among each of the three metals overlap, structural and spectral analysis indicates that GSH coordination is distinct for each metal.

When the cysteine thiol is deprotonated, each of the metals in this study forms structures that coordinate with the sulfur. Zn^{2+} coordination with the deprotonated thiol site on cysteine (Cys) was also reported in a previous IRMPD study.[53] Results from that study indicate that the metal coordinates in a [N,CO,S^-] fashion, consistent with the systems studied here. Both studies indicate that the deprotonation site is located at the sulfur, while the additional complexity of the GSH compared to Cys provides additional accessible coordination sites. This finding offers information related to how heavy metal ions coordinate with glutathione. It is well known[1-2, 5-14] that the thiol of the cysteine residue is the active site for the redox chemistry of glutathione. The redox capability of glutathione is dependent upon the ability of the thiol group to donate the hydrogen to reduce reactive oxygen species. Consequently, donation of the hydrogen leaves the sulfur atom free to either bind directly to heavy metals for subsequent elimination from the body or leaves the sulfur atom vulnerable to forming disulfide bridges with other oxidized glutathione molecules. Formation of the glutathione dimer, GSSG, renders glutathione unable to perform its necessary functions to manage oxidative stress and maintain homeostasis, and Cu^{2+} has been shown to oxidize GSH to form a Cu-GSSG complex.[12] Future IRMPD spectroscopy studies focusing on the coordination of

other biologically relevant heavy metals to GSH and to the oxidized dimer, GSSG, will be helpful in establishing more concrete comparisons and trends related to metal complexation with GSH and would likely reveal more information regarding how glutathione directly eliminates heavy metals from the body. The comparisons of the present gas-phase experiments to observations made in prior solution-phase studies show strong promise that gas-phase studies may offer fundamental structural information that can be directly applied to the condensed phase and used to deduce mechanisms governing biological processes.

Acknowledgement. This work was funded by the National Science Foundation, Grant CHE-2313553. The authors acknowledge the *Nederlandse Organisatie voor Wetenschappelijk Onderzoek* (NWO) for the support of the FELIX Laboratory. The Center for High Performance Computing at the University of Utah provided a generous number of computational resources to make this work possible. EHP would like to thank the NSF MPS Ascend Fellowship for support, Grant CHE-2316669.

Electronic Supplementary Information (ESI) available: Additional figures show the full experimental spectra for the FELIX experiments on $Zn(GSH-H)^+$, $Cu(GSH-H)^+$, and $Fe(GSH-H)^+$ and comparison figures of the experimental spectra for each of the systems with calculated spectra at various levels of theory. Tables of all of the products monitored for each of the FELIX experiments, additional calculated structures not discussed in the main text, the relative enthalpies at 0 K and 298 K for each of the structures discussed in the main text calculated at several levels of theory, and the experimental vibrations and the corresponding motions calculated at the MP2/6-311+G(d,p) level of theory.

References

1. Meister, A.; Anderson, M. E., Glutathione. *Annu. Rev. Biochem.* **1983,** *52* (1), 711-760.
2. Jefferies, H.; Coster, J.; Khalil, A.; Bot, J.; McCauley, R. D.; Hall, J. C., Glutathione. *ANZ J. Surgery* **2003,** *73* (7), 517-522.

3. Bakan, N.; Taysi, S.; Yilmaz, Ö.; Bakan, E.; Kuşkay, S.; Uzun, N.; Gündoğdu, M., Glutathione peroxidase, glutathione reductase, Cu–Zn superoxide dismutase activities, glutathione, nitric oxide, and malondialdehyde concentrations in serum of patients with chronic lymphocytic leukemia. *Clin. Chim. Acta* **2003,** *338* (1-2), 143-149.
4. Bandmann, O.; Weiss, K. H.; Kaler, S. G., Wilson's disease and other neurological copper disorders. *The Lancet Neurology* **2015,** *14* (1), 103-113.
5. Berndt, C.; Lillig, C. H., Glutathione, glutaredoxins, and iron. *Antioxid. Redox Signaling* **2017,** *27* (15), 1235-1251.
6. Jozefczak, M.; Remans, T.; Vangronsveld, J.; Cuypers, A., Glutathione is a key player in metal-induced oxidative stress defenses. *Int. J. Mol. Sci.* **2012,** *13* (3), 3145-3175.
7. Pearson, S. A.; Cowan, J. A., Glutathione-coordinated metal complexes as substrates for cellular transporters. *Metallomics* **2021,** *13* (5).
8. Rubino, F. M., Toxicity of Glutathione-Binding Metals: A Review of Targets and Mechanisms. *Toxics* **2015,** *3* (1), 20-62.
9. Delalande, O.; Desvaux, H.; Godat, E.; Valleix, A.; Junot, C.; Labarre, J.; Boulard, Y., Cadmium–glutathione solution structures provide new insights into heavy metal detoxification. *The FEBS journal* **2010,** *277* (24), 5086-5096.
10. Fuhr, B. J.; Rabenstein, D. L., Nuclear magnetic resonance studies of the solution chemistry of metal complexes. IX. Binding of cadmium, zinc, lead, and mercury by glutathione. *J. Am. Chem. Soc.* **1973,** *95* (21), 6944-6950.
11. Ngamchuea, K.; Batchelor-McAuley, C.; Compton, R. G., The copper (ii)-catalyzed oxidation of glutathione. *Chem. Eur. J.* **2016,** *22* (44), 15937-15944.
12. Eteshola, E. O.; Haupt, D. A.; Koos, S. I.; Siemer, L. A.; Morris Jr, D. L., The role of metal ion binding in the antioxidant mechanisms of reduced and oxidized glutathione in metal-mediated oxidative DNA damage. *Metallomics* **2020,** *12* (1), 79-91.
13. Freedman, J. H.; Ciriolo, M. R.; Peisach, J., The role of glutathione in copper metabolism and toxicity. *J. Biol. Chem.* **1989,** *264* (10), 5598-5605.
14. Krezel, A.; Bal, W., Coordination chemistry of glutathione. *Acta Biochim. Pol.* **1999,** *46* (3), 567-580.
15. Banu, L.; Blagojevic, V.; Bohme, D. K., Dissociations of gas-phase complexes of deprotonated glutathione with Co^{2+}, Ni^{2+}, Cu^{2+} and Zn^{2+}: The importance of metal ion reduction. *Int. J. Mass Spectrom.* **2013,** *345-347*, 142-152.
16. Gregori, B.; Guidoni, L.; Chiavarino, B.; Scuderi, D.; Nicol, E.; Frison, G.; Fornarini, S.; Crestoni, M. E., Vibrational Signatures of S-Nitrosoglutathione as Gaseous, Protonated Species. *J. Phys. Chem. B* **2014,** *118* (43), 12371-12382.
17. Maret, W., The redox biology of redox-inert zinc ions. *Free Radic Biol Med* **2019,** *134*, 311-326.
18. Lehninger, A. L.; Nelson, D. L.; Cox, M. M., *Lehninger principles of biochemistry*. Macmillan: 2005.
19. Campbell, S.; Beauchamp, J. L.; Rempe, M.; Lichtenberger, D. L., Correlations of lone pair ionization energies with proton affinities of amino acids and related compounds. Site specificity of protonation. *Int. J. Mass Spectrom. Ion Processes* **1992,** *117*, 83-99.
20. Harrison, A. G., The Gas-Phase Basicities and Proton Affinities of Amino Acids and Peptides. *Mass Spectrom. Rev.* **1997,** *16*, 201-221.
21. Fridgen, T. D., Infrared consequence spectroscopy of gaseous protonated and metal ion cationized complexes. *Mass Spectrom. Rev.* **2009,** *28* (4), 586-607.

22. Rajabi, K.; Fridgen, T. D., Structures of Aliphatic Amino Acid Proton-Bound Dimers by Infrared Multiple Photon Dissociation Spectroscopy in the 700-2000 cm^{-1} Region. *J. Phys Chem. A* **2008,** *112*, 23-30.
23. Kempkes, L. J. M.; Martens, J.; Berden, G.; Oomens, J., Dehydration reactions of protonated dipeptides containing asparagine or glutamine investigated by infrared ion spectroscopy. *Int. J. Mass Spectrom.* **2018,** *429*, 90-100.
24. Boles, G. C.; Kempkes, L. J. M.; Martens, J.; Berden, G.; Oomens, J.; Armentrout, P. B., Ion Spectroscopy and Guided Ion Beam Studies of Protonated Asparaginyl-Threonine Decomposition: Influence of a Hydroxyl Containing C-Terminal Residue on Deamidation Processes. *Int. J. Mass Spectrom.* **2019,** *442*, 64-82.
25. Boles, G. C.; Owen, C. J.; Berden, G.; Oomens, J.; Armentrout, P. B., Experimental and Theoretical Investigations of Infrared Multiple Photon Dissociation Spectra of Glutamic Acid Complexes with Zn^{2+} and Cd^{2+}. *Phys. Chem. Chem. Phys.* **2017,** *19*, 12394 - 12406.
26. Hofstetter, T. E.; Howder, C.; Berden, G.; Oomens, J.; Armentrout, P. B., Structural Elucidation of Biological and Toxicological Complexes: Investigation of Monomeric and Dimeric Complexes of Histidine with Multiply Charged Transition Metal (Zn and Cd) Cations using IR Action Spectroscopy. *J. Phys. Chem. B* **2011,** *115* (43), 12648-12661.
27. Stevenson, B. C.; Peckelsen, K.; Martens, J.; Berden, G.; Oomens, J.; Schäfer, M.; Armentrout, P. B., An investigation of inter-ligand coordination and flexibility: IRMPD spectroscopic and theoretical evaluation of calcium and nickel histidine dimers. *J. Mol. Spectrosc.* **2021,** *381*, 111532.
28. Owen, C. J.; Boles, G. C.; Berden, G.; Oomens, J.; Armentrout, P. B., Experimental and Theoretical Investigations of Infrared Multiple Photon Dissociation Spectra of Lysine Complexes with Zn^{2+} and Cd^{2+}. *Eur. J. Mass Spectrom.* **2019,** *25*, 97-111.
29. Gillis, E. A. L.; Rajabi, K.; Fridgen, T. D., Structures of Hydrated Li^+−Thymine and Li^+−Uracil Complexes by IRMPD Spectroscopy in the N−H/O−H Stretching Region. *J. Phys. Chem. A* **2009,** *113* (5), 824-832.
30. Rajabi, K.; Gillis, E. A. L.; Fridgen, T. D., Structures of Alkali Metal Ion−Adenine Complexes and Hydrated Complexes by IRMPD Spectroscopy and Electronic Structure Calculations. *J. Phys. Chem. A* **2010,** *114* (10), 3449-3456.
31. Nei, Y.-w.; Akinyemi, T. E.; Kaczan, C. M.; Steill, J. D.; Berden, G.; Oomens, J.; Rodgers, M. T., Infrared multiple photon dissociation action spectroscopy of sodiated uracil and thiouracils: Effects of thioketo-substitution on gas-phase conformation. *Int. J. Mass Spectrom.* **2011,** *308*, 191-202.
32. Yang, B.; Wu, R. R.; Polfer, N. C.; Berden, G.; Oomens, J.; Rodgers, M. T., IRMPD Action Spectroscopy of Alkali Metal Cation–Cytosine Complexes: Effects of Alkali Metal Cation Size on Gas Phase Conformation. *J. Am. Soc. Mass Spectrom.* **2013,** *24* (10), 1523-1533.
33. Kaczan, C. M.; Rathur, A. I.; Wu, R. R.; Chen, Y.; Austin, C. A.; Berden, G.; Oomens, J.; Rodgers, M. T., Infrared multiple photon dissociation action spectroscopy of sodium cationized halouracils: Effects of sodium cationization and halogenation on gas-phase conformation. *Int. J. Mass Spectrom.* **2015,** *378*, 76-85.
34. Corinti, D.; Maccelli, A.; Chiavarino, B.; Maitre, P.; Scuderi, D.; Bodo, E.; Fornarini, S.; Crestoni, M. E., Vibrational signatures of curcumin's chelation in copper(II) complexes: An appraisal by IRMPD spectroscopy *J. Chem. Phys.* **2019,** *150* (16).

35. Polfer, N. C.; Oomens, J.; Moore, D. T.; von Helden, G.; Meijer, G.; Dunbar, R. C., Infrared Spectroscopy of Phenylalanine Ag(I) and Zn(II) Complexes in the Gas Phase. *J. Am. Chem. Soc.* **2006,** *128*, 517-525.
36. Polfer, N. C.; Oomens, J.; Dunbar, R. C., IRMPD Spectroscopy of Metal-Ion/Tryptophan Complexes. *Phys. Chem. Chem. Phys.* **2006,** *8*, 2744-2751.
37. Forbes, M. W.; Bush, M. F.; Polfer, N. C.; Oomens, J.; Dunbar, R. C.; Williams, E. R.; Jockusch, R. A., Infrared Spectroscopy of Arginine Cation Complexes: Direct Observation of Gas-Phase Zwitterions. *J. Phys. Chem. A* **2007,** *111*, 11759-11770.
38. Bush, M. F.; Forbes, M. W.; Jockusch, R. A.; Oomens, J.; Polfer, N. C.; Saykally, R. J.; Williams, E. R., Infrared Spectroscopy of Cationized Lysine and ε-N-methyllysine in the Gas Phase: Effects of Alkali-Metal Ion Size and Proton Affinity on Zwitterion Stability. *J. Phys. Chem. A* **2007,** *111* (32), 7753-7760.
39. Bush, M. F.; Oomens, J.; Saykally, R. J.; Williams, E. R., Alkali Metal Ion Binding to Glutamine and Glutamine Derivatives Investigated by Infrared Action Spectroscopy and Theory. *J. Phys. Chem. A* **2008,** *112*, 8578-8584.
40. Bush, M. F.; Oomens, J.; Saykally, R. J.; Williams, E. R., Effects of Alkaline Earth Metal Ion Complexation on Amino Acid Zwitterion Stability: Results from Infrared Action Spectroscopy. *J. Am. Chem. Soc.* **2008,** *130*, 6463-6471.
41. Rodgers, M. T.; Armentrout, P. B.; Oomens, J.; Steill, J. D., Infrared Multiphoton Dissociation Spectroscopy of Cationized Threonine: Effects of Alkali-Metal Cation Size on Gas-Phase Conformation. *J. Phys. Chem. A* **2008,** *112*, 2258-2267.
42. Drayss, M. K.; Blunk, D.; Oomens, J.; Schäfer, M., Infrared Multiple Photon Dissociation Spectroscopy of Potassiated Proline. *J. Phys Chem. A* **2008,** *112*, 11972-11974.
43. Bush, M. F.; Oomens, J.; Williams, E. R., Proton Affinity and Zwitterion Stability: New Results from Infrared Spectroscopy and Theory of Cationized Lysine and Analogues in the Gas Phase. *J. Phys. Chem. A* **2009,** *113*, 431-438.
44. Heaton, A. L.; Bowman, V. N.; Oomens, J.; Steill, J. D.; Armentrout, P. B., Infrared Multiple Photon Dissociation Spectroscopy of Cationized Asparagine: Effects of Metal Cation Size on Gas-Phase Conformation. *J. Phys. Chem. A* **2009,** *113* (19), 5519-5530.
45. Dunbar, R. C.; Steill, J. D.; Oomens, J., Cationized phenylalanine conformations characterized by IRMPD and computation for singly and doubly charged ions. *Phys. Chem. Chem. Phys.* **2010,** *12* (41), 13383-13393.
46. Drayss, M. K.; Armentrout, P. B.; Oomens, J.; Schäfer, M., IR Spectroscopy of Cationized Aliphatic Amino Acids: Stability of Charge-solvated Structure Increases with Metal Cation Size. *Int. J. Mass Spectrom.* **2010,** *297*, 18–27.
47. Carl, D. R.; Cooper, T. E.; Oomens, J.; Steill, J. D.; Armentrout, P. B., Infrared Multiple Photon Dissociation Spectroscopy of Cationized Methionine: Effects of Alkali-Metal Cation Size on Gas-Phase Conformation. *Phys. Chem. Chem. Phys.* **2010,** *12*, 3384-3398.
48. Citir, M.; Stennett, E. M. S.; Oomens, J.; Steill, J. D.; Rodgers, M. T.; Armentrout, P. B., Infrared Multiple Photon Dissociation Spectroscopy of Cationized Cysteine: Effects of Metal Cation Size on Gas-Phase Conformation. *Int. J. Mass Spectrom.* **2010,** *297*, 9-17.
49. Burt, M. B.; Decker, S. G. A.; Atkins, C. G.; Rowsell, M.; Peremans, A.; Fridgen, T. D., Structures of Bare and Hydrated $[Pb(AminoAcid-H)]^+$ Complexes Using Infrared Multiple Photon Dissociation Spectroscopy. *J. Phys. Chem. B* **2011,** *115* (39), 11506-11518.

50. Citir, M.; Hinton, C. S.; Oomens, J.; Steill, J. D.; Armentrout, P. B., Infrared Multiple Photon Dissociation Spectroscopy of Cationized Histidine: Effects of Metal Cation Size on Gas-Phase Conformation. *J. Phys. Chem. A* **2012,** *116*, 1532-1541.
51. Gholami, A.; Fridgen, T. D., Structures and Unimolecular Reactivity of Gas-Phase $[Zn(Proline-H)]^+$ and $[Zn(Proline-H)(H_2O)]^+$. *J. Phys. Chem. B* **2013,** *117*, 8447-8456.
52. Boles, G. C.; Coates, R. A.; Berden, G.; Oomens, J.; Armentrout, P. B., Experimental and Theoretical Investigations of Infrared Multiple Photon Dissociation Spectra of Glutamine Complexes with Zn^{2+} and Cd^{2+}. *J. Phys. Chem. B* **2015,** *119*, 11607–11617.
53. Coates, R. A.; McNary, C. P.; Boles, G. C.; Berden, G.; Oomens, J.; Armentrout, P. B., Structural Characterization of Gas-Phase Cysteine and Cysteine Methyl Ester Complexes with Zinc and Cadmium Dications by Infrared Multiple Photon Dissociation Spectroscopy. *Phys. Chem. Chem. Phys.* **2015,** *17*, 25799-25808.
54. Coates, R. A.; Boles, G. C.; McNary, C. P.; Berden, G.; Oomens, J.; Armentrout, P. B., Zn^{2+} and Cd^{2+} Cationized Serine Complexes: Infrared Multiple Photon Dissociation Spectroscopy and Density Functional Theory Investigations. *Phys. Chem. Chem. Phys.* **2016,** *18*, 22434 – 22445.
55. Boles, G. C.; Coates, R. A.; Berden, G.; Oomens, J.; Armentrout, P. B., Experimental and Theoretical Investigations of Infrared Multiple Photon Dissociation Spectra of Asparagine Complexes with Zn^{2+} and Cd^{2+} and Their Deamidation Processes. *J. Phys. Chem. B* **2016,** *120*, 12486-12500.
56. Boles, G. C.; Hightower, R. L.; Coates, R. A.; McNary, C. P.; Berden, G.; Oomens, J.; Armentrout, P. B., Experimental and Theoretical Investigations of Infrared Multiple Photon Dissociation Spectra of Aspartic Acid Complexes with Zn^{2+} and Cd^{2+}. *J. Phys. Chem. B* **2018,** *122*, 3836-3853.
57. Chalifoux, A. M.; Boles, G. C.; Berden, G.; Oomens, J.; Armentrout, P. B., Experimental and Theoretical Investigations of Infrared Multiple Photon Dissociation Spectra of Arginine Complexes with Zn^{2+} and Cd^{2+}. *Phys. Chem. Chem. Phys.* **2018,** *20*, 20712-20725.
58. Boles, G. C.; Hightower, R. L.; Berden, G.; Oomens, J.; Armentrout, P. B., Zinc and Cadmium Complexation of l-Threonine: An Infrared Multiple Photon Dissociation Spectroscopy and Theoretical Study. *J. Phys. Chem. B* **2019,** *123* (44), 9343-9354.
59. Boles, G. C.; Stevenson, B. C.; Hightower, R. L.; Berden, G.; Oomens, J.; Armentrout, P. B., Zinc and cadmium complexation of L-methionine: An infrared multiple photon dissociation spectroscopy and theoretical study. *J. Mass Spectrom.* **2021,** *56* (4), e4580.
60. Armentrout, P. B.; Boles, G. C.; Ghiassee, M.; Berden, G.; Oomens, J., Infrared Multiple-Photon Dissociation Spectra of Sodiated Complexes of the Aliphatic Amino Acids. *J. Phys. Chem. A* **2021,** *125* (29), 6348-6355.
61. Armentrout, P. B.; Armentrout, E. I.; Clark, A. A.; Cooper, T. E.; Stennett, E. M. S.; Carl, D. R., An Experimental and Theoretical Study of Alkali Metal Cation Interactions with Cysteine. *J. Phys. Chem. B* **2010,** *114* (11), 3927-3937.
62. Stevenson, B. C.; Martens, J.; Berden, G.; Oomens, J.; Armentrout, P. B., Spectroscopic Investigation of the Metal Coordination of the Aromatic Amino Acids with Zinc and Cadmium. *J. Phys. Chem. A* **2023,** *127*, 3560-3569.
63. Polfer, N. C.; Oomens, J.; Dunbar, R. C., Alkali metal complexes of the Dipeptides PheAla and AlaPhe : IRMPD spectroscopy. *ChemPhysChem* **2008,** *9*, 579-589.

64. Prell, J. S.; Demireva, M.; Oomens, J.; Williams, E. R., Role of Sequence in Salt-Bridge Formation for Alkali Metal Cationized GlyArg and ArgGly Investigated with IRMPD Spectroscopy and Theory. *J. Am. Chem. Soc.* **2009,** *131*, 1232-1242.
65. Stevenson, B. C.; Berden, G.; Martens, J.; Oomens, J.; Armentrout, P. B., Determining gas-phase chelation of zinc, cadmium, and copper cations with HisHis dipeptide using action spectroscopy and theoretical calculations. *Int. J. Mass Spectrom.* **2024,** *495*, 117154.
66. Kullman, M. J.; Molesworth, S. P.; Berden, G.; Oomens, J.; Van Stipdonk, M., IRMPD spectroscopy b_2 ions from protonated tripeptides with 4-aminomethyl benzoic acid residues. *Int. J. Mass Spectrom.* **2012,** *316-318*, 174-181.
67. Dunbar, R. C.; Martens, J.; Berden, G.; Oomens, J., Complexes of Ni(II) and Cu(II) with small peptides: deciding whether to deprotonate. *Phys. Chem. Chem. Phys.* **2016,** *18* (38), 26923-26932.
68. Dunbar, R. C.; Martens, J.; Berden, G.; Oomens, J., Transition Metal(II) Complexes of Histidine-containing Tripeptides: Structures, and Infrared Spectroscopy by IRMPD. *Int. J Mass Spectrom.* **2018,** *429*, 198-205.
69. Dunbar, R. C.; Steill, J. D.; Polfer, N. C.; Oomens, J., Dimeric Complexes of Tryptophan with M^{2+} Metal Ions. *J. Phys. Chem. A* **2009,** *113* (5), 845-851.
70. Stevenson, B. C.; Martens, J.; Berden, G.; Oomens, J.; Schäfer, M.; Armentrout, P. B., IRMPD Spectroscopic and Theoretical Structural Investigations of Zinc and Cadmium Dications Bound to Histidine Dimers. *J. Phys. Chem. A* **2020,** *124* (49), 10266-10276.
71. Oepts, D.; van der Meer, A. F. G.; van Amersfoort, P. W., The Free-Electron-Laser User Facility FELIX. *Infrared Phys. Technol.* **1995,** *36*, 297-308.
72. Martens, J.; Berden, G.; Gebhardt, C. R.; Oomens, J., Infrared ion spectroscopy in a modified quadrupole ion trap mass spectrometer at the FELIX free electron laser laboratory. *Rev. Sci. Instrum.* **2016,** *87* (10), 103108.
73. Berden, G.; Derksen, M.; Houthuijs, K. J.; Martens, J.; Oomens, J., An Automatic Variable Laser Attenuator for IRMPD Spectroscopy and Analysis of Power-dependence in Fragmentation Spectra. *Int. J. Mass Spectrom.* **2019,** *443*, 1-8.
74. Lemaire, J.; Boissel, P.; Heninger, M.; Mauclaire, G.; Bellec, G.; Mestdagh, H.; Le Caer, S.; Ortega, J.; Glotin, F.; Maître, P., Gas Phase Infrared Spectroscopy of Selectively Prepared Ions. *Phys. Rev. Lett.* **2002,** *89*, 273002.
75. Moision, R. M.; Armentrout, P. B., The Special Five-membered Ring of Proline: An Experimental and Theoretical Investigation of Alkali Metal Cation Interactions with Proline and Its Four- and Six-membered Ring Analogues. *J. Phys. Chem. A* **2006,** *110*, 3933-3946.
76. McNary, C. P.; Armentrout, P. B., Threshold Collision-Induced Dissociation of Proton-Bound Hydrazine and Dimethylhydrazine Clusters. *J. Phys. Chem. A* **2016,** *120*, 9690-9701.
77. McNary, C. P.; Nei, Y.-w.; Maitre, P.; Rodgers, M. T.; Armentrout, P. B., Infrared Multiple Photon Dissociation Spectroscopy of Protonated Glycine, Lysine, Histidine, and Arginine Complexed with 18-Crown-6. *Phys. Chem. Chem. Phys.* **2019,** *21*, 12625-12639.
78. Valiev, M.; Bylaska, E. J.; Govind, N.; Kowalski, K.; Straatsma, T. P.; Van Dam, H. J. J.; Wang, D.; Nieplocha, J.; Apra, E.; al., E., NWChem: A comprehensive and scalable open-source solution for large scale molecular simulations. *Comput. Phys. Commun.* **2010,** *181*, 1477-1489.
79. Pearlman, D. A.; Case, D. A.; Caldwell, J. W.; Ross, W. R.; Cheatham, T. E.; DeBolt, S.; Ferguson, D.; Seibel, G.; Kollman, P., AMBER, a computer program for applying molecular mechanics, normal mode analysis, molecular dynamics and free energy calculations to elucidate the structures and energies of molecules. *Comp. Phys. Commun.* **1995,** *91*, 1-41.

80. Case, D. A.; Babin, V.; Berryman, J. T.; Betz, R. M.; Cai, Q.; Cerutti, D. S.; Cheatham, T. E.; Darden, T. A.; Duke, R. E.; Gohlke, H.; Goetz, A. W.; Gusarov, S.; Homeyer, N.; Janowski, P.; Kaus, J.; Kolossváry, I.; Kovalenko, A.; Lee, T. S.; LeGrand, S.; Luchko, T.; Luo, R.; Madej, B.; Merz, K. M.; Paesani, F.; Roe, D. R.; Roitberg, A.; Sagui, C.; Salomon-Ferrer, R.; Seabra, G.; Simmerling, C. L.; Smith, W.; Swails, J.; Walker, R. C.; Wang, J.; Wolf, R. M.; Wu, X.; Kollman, P. A. *AMBER 14*, University of California: San Francisco, 2014.
81. Spezia, R.; Tournois, G.; Tortajada, J.; Cartailler, T.; Gaigeot, M.-P., Toward a DFT-based molecular dynamics description of Co(II) binding in sulfur-rich peptides. *Phys. Chem. Chem. Phys.* **2006,** *8* (17), 2040-2050.
82. Becke, A. D., Density-functional Thermochemistry. III. The Role of Exact Exchange. *J. Chem. Phys.* **1993,** *98*, 5648-5652.
83. Lee, C.; Yang, W.; Parr, R. G., Development of the Colle-Salvetti Correlation-Energy Formula into a Functional of the Electron Density. *Phys. Rev. B* **1988,** *37*, 785-789.
84. Frisch, M. J.; Trucks, G. W.; Schlegel, H. B.; Scuseria, G. E.; Robb, M. A.; Cheeseman, J. R.; Scalmani, G.; Barone, V.; Petersson, G. A.; Nakatsuji, H.; Li, X.; Caricato, M.; Marenich, A. V.; Bloino, J.; Janesko, B. G.; Gomperts, R.; Mennucci, B.; Hratchian, H. P.; Ortiz, J. V.; Izmaylov, A. F.; Sonnenberg, J. L.; Williams-Young, D.; Ding, F.; Lipparini, F.; Egidi, F.; Goings, J.; Peng, B.; Petrone, A.; Henderson, T.; Ranasinghe, D.; Zakrzewski, V. G.; Gao, J.; Rega, N.; Zheng, G.; Liang, W.; Hada, M.; Ehara, M.; Toyota, K.; Fukuda, R.; Hasegawa, J.; Ishida, M.; Nakajima, T.; Honda, Y.; Kitao, O.; Nakai, H.; Vreven, T.; Throssell, K.; J. A. Montgomery, J.; Peralta, J. E.; Ogliaro, F.; Bearpark, M. J.; Heyd, J. J.; Brothers, E. N.; Kudin, K. N.; Staroverov, V. N.; Keith, T. A.; Kobayashi, R.; Normand, J.; Raghavachari, K.; Rendell, A. P.; Burant, J. C.; Iyengar, S. S.; Tomasi, J.; Cossi, M.; Millam, J. M.; Klene, M.; Adamo, C.; Cammi, R.; Ochterski, J. W.; Martin, R. L.; Morokuma, K.; Farkas, O.; Foresman, J. B.; Fox, D. J. *Gaussian 16, Revision A.03*, Gaussian, Inc.: Wallingford CT, 2016.
85. Möller, C.; Plesset, M. S., Note on an Approximation Treatment for Many-Electron Systems. *Phys. Rev.* **1934,** *46*, 618-622.
86. Polfer, N. C., Infrared Multiple Photon Dissociation Spectroscopy of Trapped Ions. *Chem. Soc. Rev.* **2011,** *40*, 2211−2221.
87. Mardirossian, N.; Head-Gordon, M., ωB97M-V: A combinatorially optimized, range-separated hybrid, meta-GGA density functional with VV10 nonlocal correlation. *J. Chem. Phys.* **2016,** *144* (21), 214110.
88. Kesharwani, M. K.; Brauer, B.; Martin, J. M. L., Frequency and Zero-Point Vibrational Energy Scale Factors for Double-Hybrid Density Functionals (and Other Selected Methods): Can Anharmonic Force Fields Be Avoided? *J. Phys. Chem. A* **2015,** *119* (9), 1701-1714.
89. Grimme, S.; Antony, J.; Ehrlich, S.; Krieg, H., A Consistent and Accurate Ab Initio Parametrization of Density Functional Dispersion Correction (DFT-D) for the 94 Elements H-Pu. *J. Chem. Phys.* **2010,** *132* (15), 154104-154119.
90. Grimme, S.; Ehrlich, S.; Goerigk, L., Effect of the Damping Function in Dispersion Corrected Density Functional Theory. *J. Comput. Chem.* **2011,** *32* (7), 1456-1465.
91. Dunbar, R. C.; Berden, G.; Oomens, J., How does a small peptide choose how to bind a metal ion? IRMPD and computational survey of CS versus Iminol binding preferences. *Int. J. Mass Spectrom.* **2013,** *354-355*, 356-364.
92. Walker, S. K.; Stevenson, B. C.; Yang, F.; Jones, R. M.; Berden, G.; Martens, J.; Oomens, J.; Armentrout, P. B., Structural characterizations of histidine-containing tripeptides

complexed with zinc and cadmium dications using IRMPD spectroscopy and theoretical calculations. *Int. J. Mass Spectrom.* **2024,** *503*, 117281.
93. Oomens, J.; Tielens, A. G. G. M.; Sartakov, B. G.; von Helden, G.; Meijer, G., Laboratory Infrared Spectroscopy of Cationic Polycyclic Aromatic Hydrocarbon Molecules. *Astrophys. J.* **2003,** *591* (2), 968.

Table 1. Comparison of metal-ligand bond distances for each of the systems discussed at MP2 level of theory.

Zinc Binding Motif	Metal-Ligand Bond Distance (Å)
[N^1, CO^{γ}, S^-, CO^3]	[2.06, 2.02, 2.22, 2.05]
[N^1, CO^1, CO^{γ}, CO^{3-}]	[2.05, 2.09, 2.02, 1.86]
[CO^1, CO^{γ}, S^-, CO^3]	[2.02, 2.02, 2.21, 2.05]
[N^1, CO^1, N^2H, S^-]	[2.09, 2.12, 2.16, 2.17]
Copper Binding Motif	**Metal-Ligand Bond Distance**
[N^1, CO^1, N^2H, S^-]	[2.06, 1.99, 2.22, 2.14]
[N^1, S^-, CO^2]	[1.97, 2.16, 1.95]
[N^1, CO^{γ}, S^-, N^3H, CO^3]	[1.99, 2.20, 2.23, 2.10, 2.07]
[N^1, CO^1, N^2, S^-, CO^3]	[2.02, 2.11, 2.27, 2.23, 1.99]
Fe Quintet Binding Motif	**Metal-Ligand Bond Distance**
[CO^1, S^-, CO^2, CO^3]	[2.00, 2.29, 2.11, 2.17]
[CO^1, CO^{γ}, S^-, CO^3]	[2.07, 2.06, 2.30, 2.13]
[N^1, CO^1, N^2, S^-, CO^2]	[2.19, 2.27, 2.16, 2.32, 2.13]
[N^1, N^2H, S^-, CO^2]	[2.13, 2.29, 2.28, 2.06]

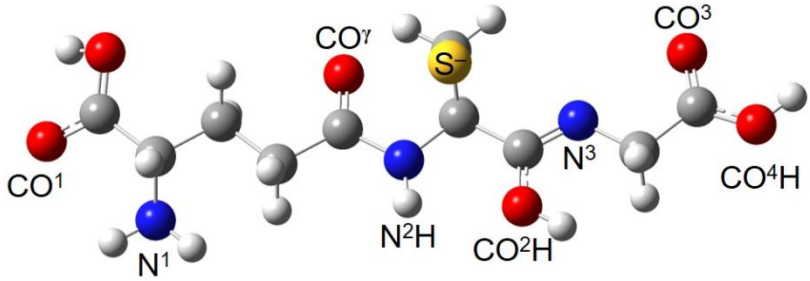

Figure 1. Detailed example of the nomenclature used to describe the metal coordination sites of glutathione. Here, GSH is deprotonated at the sulfur and the CO^2H-N^3 linkage is in its iminol form.

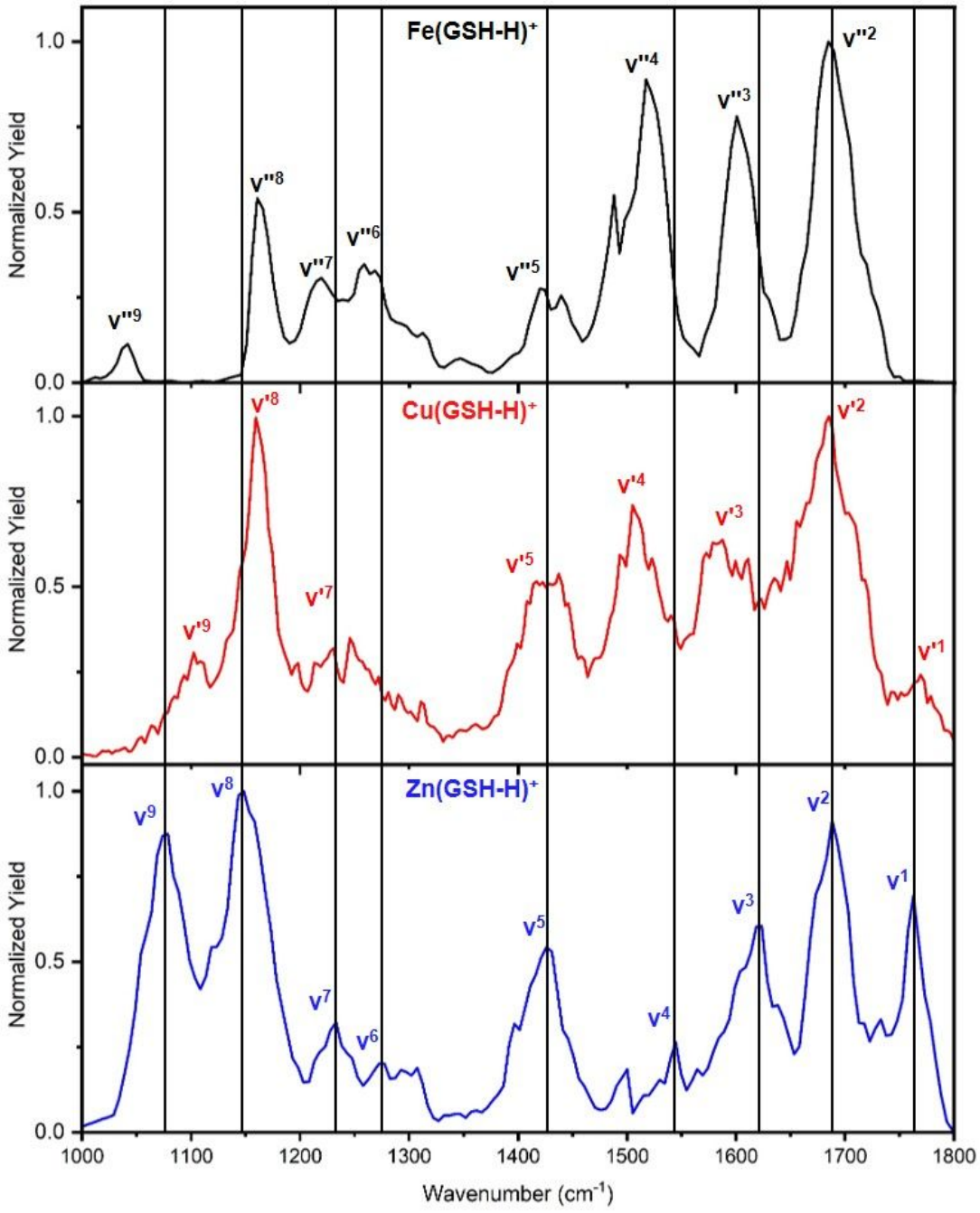

Figure 2. Comparison of the $M(GSH-H)^+$ experimental IRMPD spectra for M = Fe (black), Cu (red), and Zn (blue). Vertical lines correspond to the major peaks in the Zn system that correlate well with those observed in the Cu and Fe systems.

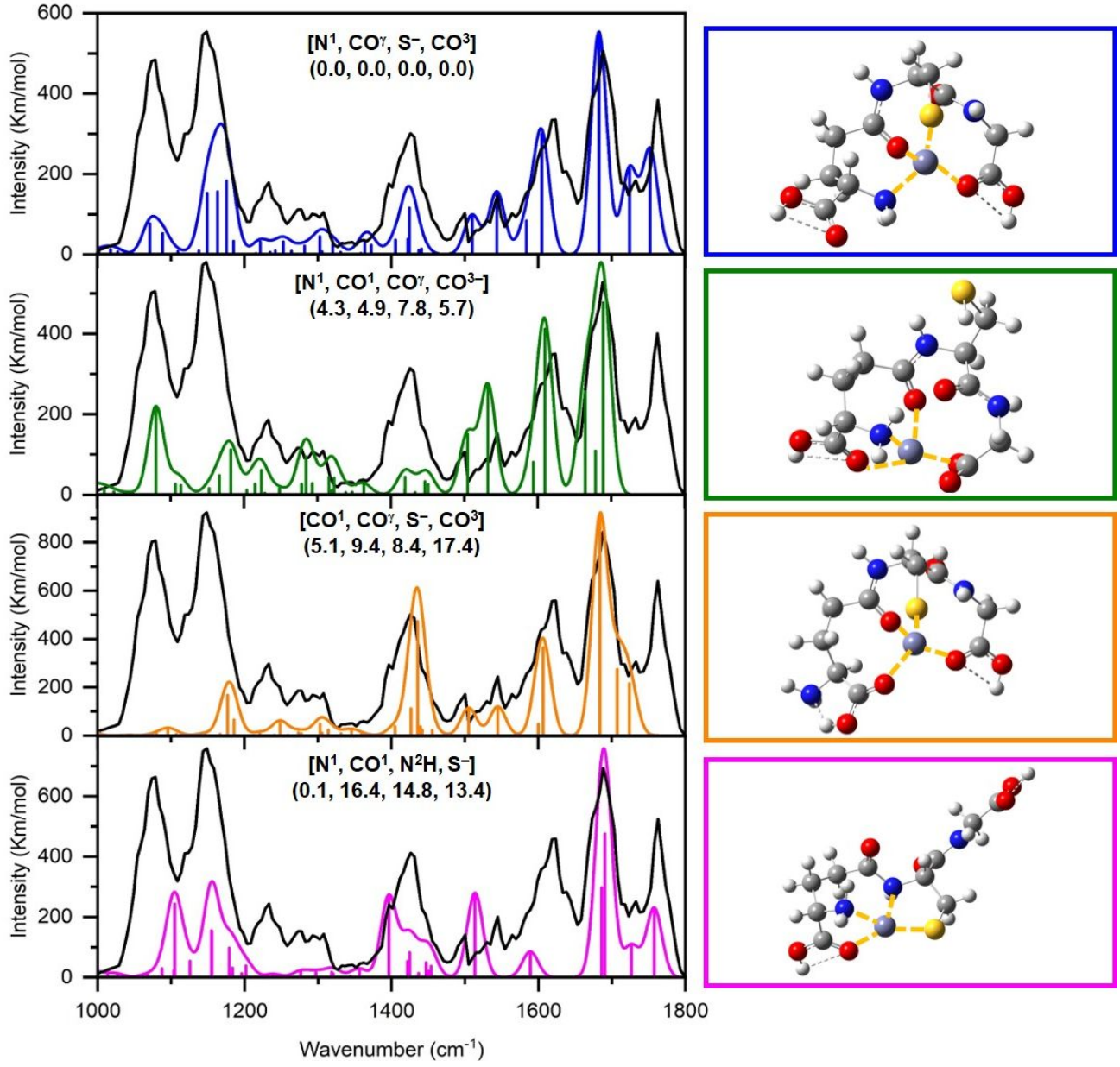

Figure 3. Comparison of the Zn(GSH-H)$^+$ experimental IRMPD spectrum (solid black line) with spectra calculated at the MP2/6-311+G(d,p) level of theory for low-lying conformers. Relative 298 K Gibbs energies (kJ/mol) are given at the B3LYP//B3LYP, B3LYP-GD3BJ//B3LYP-GD3BJ, ωB97XD//MP2, and MP2(full)//MP2 levels, respectively, using the 6-311+G(2d,2p) basis set. Structures of Zn(GSH-H)$^+$ conformers calculated at MP2/6-311+G(d,p) level of theory are shown

to the right of their calculated spectrum. Dashed lines indicate hydrogen bonds and yellow dashed lines indicate metal-ligand interactions.

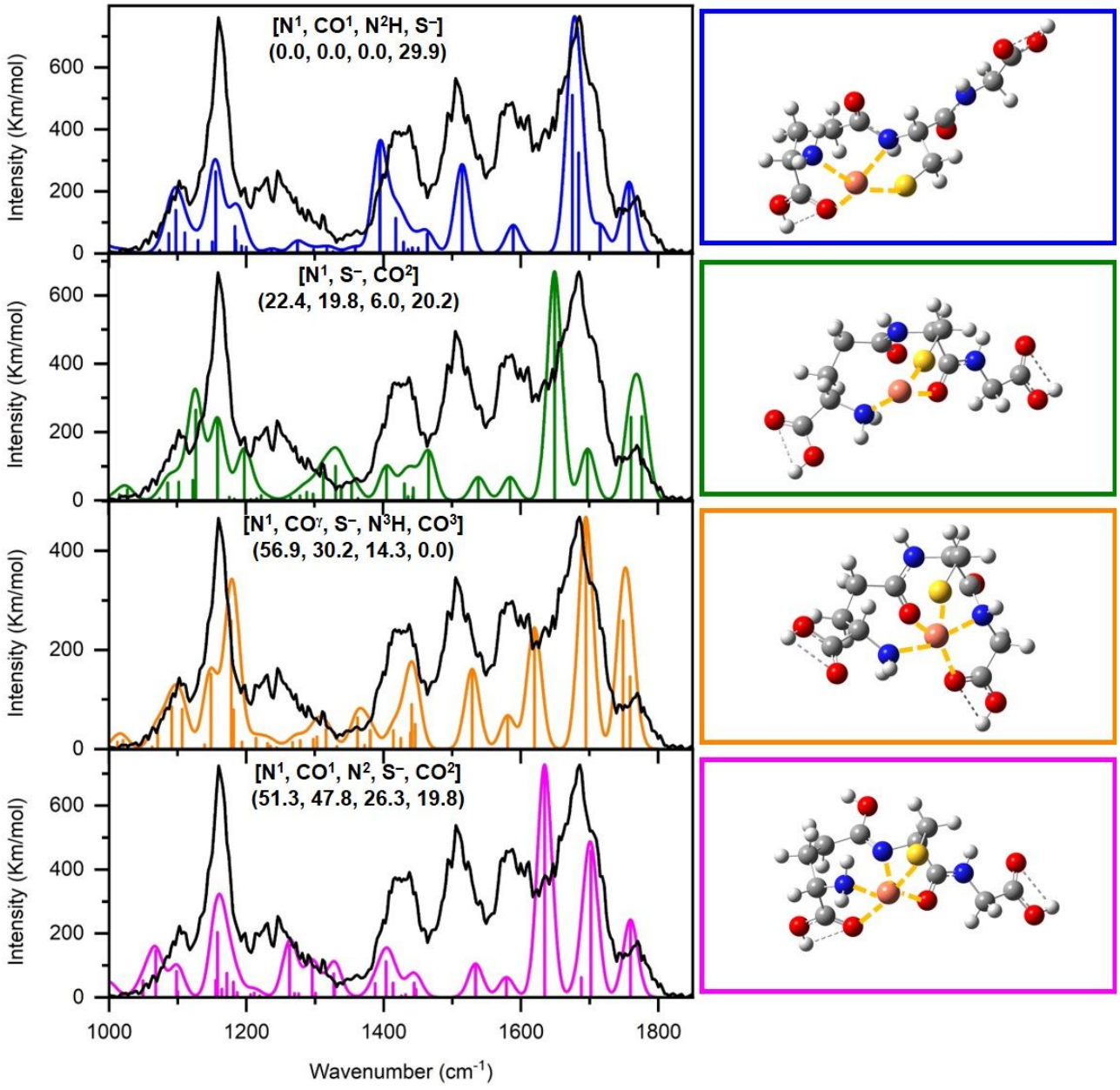

Figure 4. Comparison of the Cu(GSH-H)$^+$ experimental IRMPD spectrum (solid black line) with spectra calculated at the MP2/6-311+G(d,p) level of theory for low-lying conformers. Relative 298 K Gibbs energies (kJ/mol) are given at the B3LYP//B3LYP, B3LYP-GD3BJ//B3LYP-GD3BJ, ωB97XD//MP2, and MP2(full)//MP2 levels, respectively, using the 6-311+G(2d,2p) basis set. Structures of Cu(GSH-H)$^+$ conformers calculated at MP2/6-311+G(d,p) level of theory are shown

to the right of their calculated spectrum. Dashed lines indicate hydrogen bonds and yellow dashed lines indicate metal-ligand interactions.

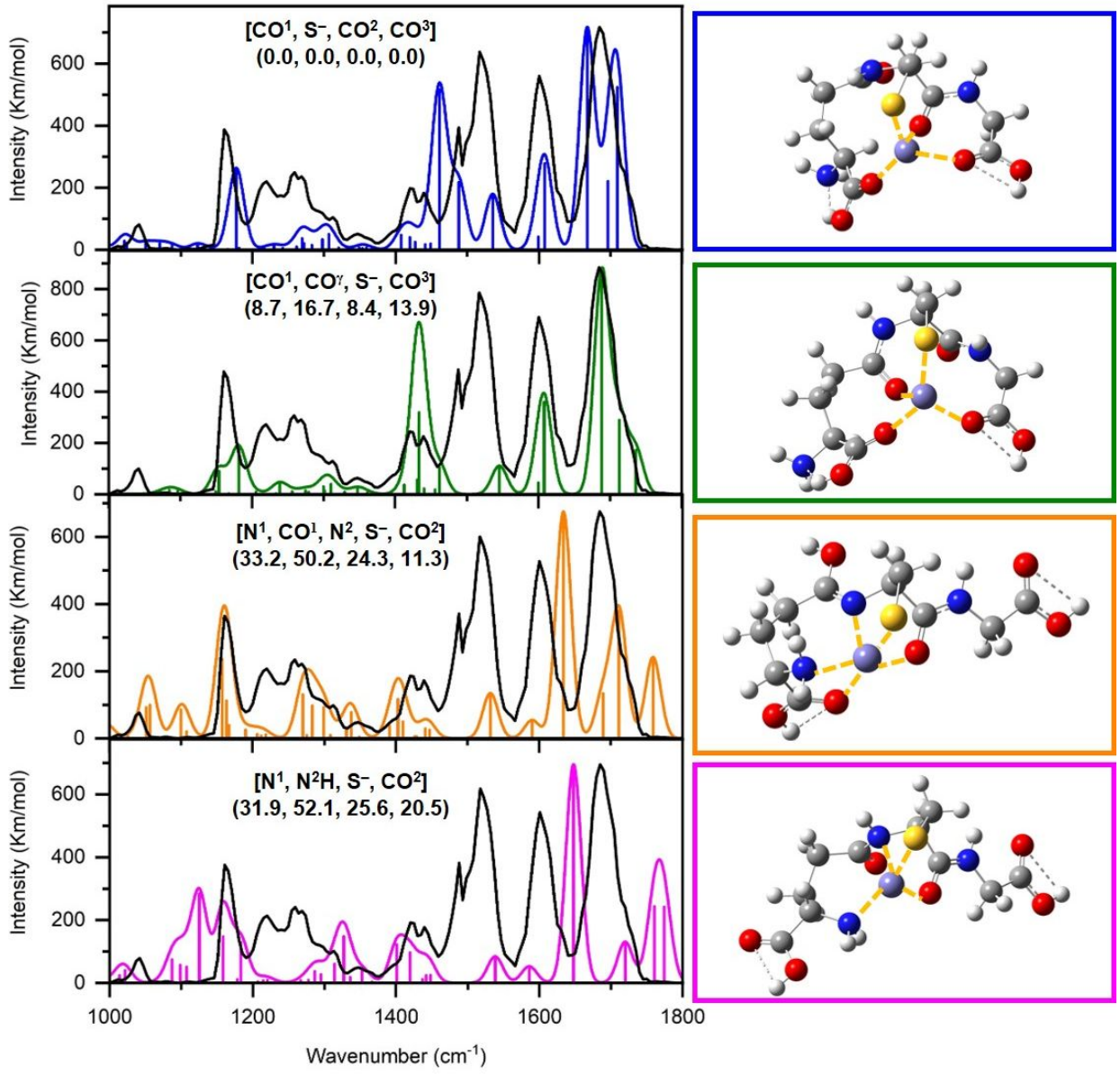

Figure 5. Comparison of the $Fe(GSH-H)^+$ experimental IRMPD spectrum (solid black line, light gray times 5) with spectra calculated at the MP2/6-311+G(d,p) level of theory for low-lying conformers. Relative 298 K Gibbs energies (kJ/mol) are given at the B3LYP//B3LYP, B3LYP-GD3BJ//B3LYP-GD3BJ, ωB97XD//MP2, and MP2(full)//MP2 levels, respectively, using the 6-311+G(2d,2p) basis set. Structures of low-lying $Fe(GSH-H)^+$ conformers with quintet spin state calculated at the MP2/6-311+G(d,p) level of theory are shown to the right of their calculated spectrum. Dashed lines indicate hydrogen bonds and yellow dashed lines indicate metal-ligand interactions.

The data supporting this article have been included either in the article or as part of the Supplementary Information.